Electronic Phase Transition and an Anomalous Ordered Phase in $Ba_2Ti_{13}O_{22}$ with $3d^1$ Ions on a Triangle-Based Lattice

K. Takayama,[1] T. Koyama,[2] S. Mori,[2] K. Kato,[3] M. Takata,[3] J. Fujioka,[4] Y. Tokura,[4] J. Miyazaki,[1] and T. Katsufuji[1,5,*]

[1]*Department of Physics, Waseda University, Tokyo 169-8555, Japan*
[2]*Department of Materials Science, Osaka Prefecture University, Sakai 599-8531, Japan*
[3]*RIKEN SPring-8 Center, Hyogo 679-5148, Japan*
[4]*Department of Applied Physics, University of Tokyo, Tokyo 113-8656, Japan*
[5]*Kagami Memorial Laboratory for Material Science and Technology, Waseda University, Tokyo 169-0051, Japan*

(Received 12 February 2013; published 7 May 2013)

We found that $Ba_2Ti_{13}O_{22}$ with Ti^{3+} ($3d^1$) ions on a triangle-based lattice exhibits a phase transition at $T_c \sim 200$ K, below which the increase of electrical resistivity and decrease of magnetic susceptibility were observed. Transmission electron microscopy and optical reflectivity measurements indicate that the low-temperature phase of the present compound shares characteristics in common with a charge-density-wave state with remnant carriers, although a commensurate wave vector of the modulation and a linear temperature dependence of the magnetic susceptibility below T_c suggest an exotic ordered state.

DOI: 10.1103/PhysRevLett.110.196405 PACS numbers: 71.45.Lr, 61.05.J−, 78.30.Er

Electrons in the t_{2g} states of d orbitals with threefold degeneracy exhibit various intriguing phenomena. One of the most prominent ones is orbital ordering, where electrons occupy specific states among the triply degenerate t_{2g} states at each site. This phenomenon is observed in various vanadates with V^{3+} ions ($3d^2$), for example, perovskite RVO_3 (R: rare earth) [1,2], spinel AV_2O_4 (A: divalent ion) [3,4], and $LiVO_2$ [5]. Recently, it has been shown that many vanadates with V^{3+} ions on triangle-based lattices exhibit V trimerization [6–8] induced by orbital ordering, where electrons at specific t_{2g} states form a spin-singlet bond at each side of the triangle [9].

In contrast to these vanadates with $3d^2$ ions, not so many compounds with $3d^1$ ions show a phase transition with orbital ordering. For example, it was shown by resonant x-ray scattering that perovskite titanates $RTiO_3$ with Ti^{3+} exhibits an orbital ordering [10], but this ordering occurs only as a crossover without any phase transition [11]. Spinel $MgTi_2O_4$ exhibits a structural phase transition around 200 K [12], and the crystal structure in the low-T phase of $MgTi_2O_4$ has been studied [13] and explained by an orbital ordering [14]. However, the details of the phase transition are still unknown, partly due to the lack of the single crystals.

In this Letter, we studied the physical properties of $Ba_2Ti_{13}O_{22}$ single crystals, in which Ti^{3+} ($3d^1$) ions form a triangle-based lattice [15,16]. We found that the compound exhibits a phase transition at $T_c \sim 200$ K, below which the electrical resistivity increases and magnetic susceptibility decreases. We investigated the change of the lattice and electronic structure by the electron diffraction and optical measurement and found that, though the low-T phase resembles a charge-density-wave state, there are several experimental results that are not consistent with such a simple picture but suggest an exotic ordered state in this compound.

The configuration of Ti ions in $Ba_2Ti_{13}O_{22}$ is shown Figs. 1(a) and 1(b). A "trilayer" structure shown in Fig. 1(a) is the building block of the crystal. Here, the first layer and the third layer of the trilayer are composed of five Ti ions in a "boat" shape, which are a part of the triangular lattice, as illustrated in Fig. 1(c). A second layer between two boat layers is composed of three Ti ions in a "bar" shape, which are located also as a part of the triangular lattice [Fig. 1(c)]. In other words, these are a trilayer slab of the face-centered-cubic lattice of the Ti ions perpendicular to the diagonal direction, from which several Ti ions are periodically missing. One trilayer and the next trilayer is shifted by half of the a (or b) lattice constant, as shown in Fig. 1(b). The average valence of Ti is +3.077; i.e., nominally, 12 out of 13 Ti ions are 3+ ($3d^1$), and the remaining one is 4+ ($3d^0$). It should be noted that $Ba_2V_{13}O_{22}$, which has the same crystal structure as the present compound but with V^{3+} ions ($3d^2$) instead of Ti^{3+}, exhibits a V trimerization with orbital ordering below 290 K [7].

We have grown single crystals of $Ba_2Ti_{13}O_{22}$ by a floating-zone method, in which the mixture of $BaTiO_3$, Ti, and TiO_2 was directly melted without presintering, and obtained crystals with a flat surface along the ab plane. We measured the electrical resistivity and Hall coefficient by a four-probe technique with indium as electrodes. The magnetic susceptibility was measured by a SQUID magnetometer. Strain measurements were performed by a conventional strain-gauge technique. Synchrotron x-ray powder diffraction measurements were performed with an incident wavelength of 0.774 77 Å at SPring-8 BL44B2 [17]. Electron diffraction experiments were carried out in the temperature window between 298 and 100 K in a JEM-2010 and JEM-2100F (for high-resolution images) transmission electron microscope. Reflectivity spectra [$R(\omega)$] were measured on the cleaved surface along the ab plane between 0.01 and 5 eV in phonon energies and

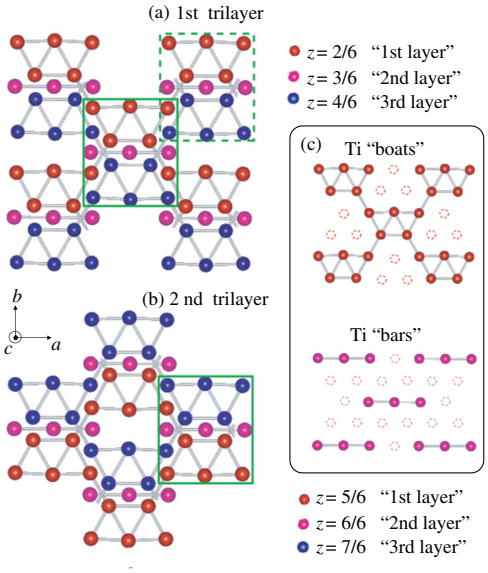

FIG. 1 (color online). (a), (b) Configuration of Ti ions in $Ba_2Ti_{13}O_{22}$ in (a) the first trilayer and (b) the second trilayer. (c) Illustrations of the boat structure (upper) and bar (lower) structure as a part of the triangular lattice. The figures of the crystal structure were drawn by VESTA [31].

between 5 and 300 K in temperatures, and the optical conductivity spectra $[\sigma(\omega)]$ and energy loss function $(\mathrm{Im}[-1/\epsilon(\omega)])$ with $\boldsymbol{E} \parallel a$ and b were obtained by the Kramers-Kronig transformation of the reflectivity spectra.

The temperature (T) dependence of electrical resistivity (ρ) is shown in Fig. 2(a) for three samples from different batches of the single crystals. As can be seen, an anomaly is observed in the resistivity along the a axis (ρ_a) at $T_c =$ 205 K for #1 and 220 K for #2, below which $\rho_a(T)$ increases. With further decreasing T, $\rho_a(T)$ decreases again and there exists an upturn below 20 K. The resistivity along the b axis (ρ_b) for #1 also exhibits a similar anomaly at $T_c = 205$ K and is approximately twice as large as ρ_a in its absolute values. The resistivity along the c axis (ρ_c) for #3 ($T_c = 205$ K) is comparable in its absolute values to ρ_a for #1.

The magnetic susceptibility $\chi(T)$ of the two samples is shown in Fig. 2(b). An anomaly is observed in $\chi(T)$ at the same temperature (T_c) where the anomaly in $\rho(T)$ is observed. Above T_c, $\chi(T)$ is almost T independent, whereas below T_c, $\chi(T)$ decreases with T almost linearly, and the values of $\chi(T)$ at the lowest temperature becomes ~70% of those above T_c. The $\chi(T)$ values along the a (χ_a) and b axis (χ_b) are almost identical, whereas those along the c axis (χ_c) are smaller than χ_a and χ_b. The absolute values of $\chi(T)$ above T_c ($\sim 1 \times 10^{-4}$ cm^3/Ti mol) is several times smaller than those of the vanadate with the same crystal structure ($Ba_2V_{13}O_{22}$, $\chi \sim 5 \times 10^{-4}$ cm^3/V mol [7]) and those of perovskite titanates with Ti^{3+} ($LaTiO_3$, $\chi \sim 5 \times 10^{-4}$ cm^3/Ti mol [18]). This suggests that the electron correlation effect in $Ba_2Ti_{13}O_{22}$ is less dominant for the electronic structure compared with those vanadates and titanates.

Figure 2(c) shows the T dependence of the Hall coefficient (R_H) for the two samples. The sign of R_H is negative at high T, whereas it changes positive and its absolute value increases with decreasing T for both samples. Anomalies are barely observed at T_c. The value of R_H at the lowest T is larger for sample #2, which has smaller values of ρ, and it corresponds to ~0.1 hole per Ti. The sign change of R_H with T suggests that both electrons and holes with different mobilities exist below T_c. According to the two-carrier model for the Hall coefficient, positive values at low T indicate that the mobility of the holes is larger than that of the electrons. Thus, the larger values of R_H at the lowest T for #2 is likely caused by the larger mobility of the holes for #2 than #1, which results in the smaller resistivity (ρ) values as shown in Fig. 2(a).

To clarify the characteristic of the phase transition from the viewpoint of the crystal structure, we performed the x-ray powder diffraction measurement on crushed $Ba_2Ti_{13}O_{22}$ crystals. However, we could not find any changes of the diffraction patterns across T_c, except for small anomalies in the lattice constants, as shown in Fig. 2(d). Similar anomalies were observed in the strain ($\Delta L/L$) measurement as shown in the inset of the same figure, where the back ground, i.e., a smooth decrease of $\Delta L/L$ with decreasing T corresponding to a normal thermal contraction, is subtracted. As can be seen, the a and c lattice constants decrease, whereas the b lattice constant increases with decreasing T below T_c.

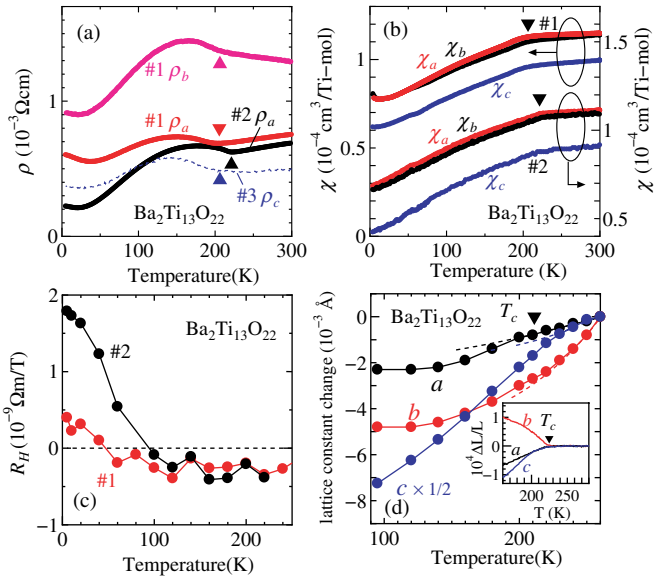

FIG. 2 (color online). Temperature dependence of (a) electrical resistivity, (b) magnetic susceptibility, (c) Hall coefficient, and (d) the change of the lattice constants for $Ba_2Ti_{13}O_{22}$. The dashed lines in (d) are guide to eyes. The inset in (d) shows the temperature dependence of strain along the three axes.

Though we could not observe a change of the diffraction patterns in the powder x-ray measurement, we detected new peaks appearing below T_c in the electron diffraction measurement: The $hk0$ peak with $h + k =$ even, as shown in Figs. 3(a) and 3(b), the $00l$ peak with $l =$ odd, and the $h0l$ peak with $l =$ odd (not shown) appear [19]. These results indicate the change of the space group from $Cmce$ to $C2/m$ [20].

With this symmetry change, the local symmetry for the cluster of the "boat-bar-boat" stacking, surrounded by a rectangle in Fig. 1(a), remains as it is. Furthermore, the C symmetry (the centered structure) also survives, and, thus, two boat-bar-boat clusters along the ab plane, surrounded by solid and dashed rectangles in Fig. 1(a), remain equivalent even in the low-T phase. However, the equivalency between a boat-bar-boat cluster on one trilayer [Fig. 1(a)] and that on the next trilayer [Fig. 1(b)] disappears in the $C2/m$ phase.

We also took high-resolution images of the transmission electron microscope. In Figs. 3(c) and 3(d), we see the alternate stacking of the bright and dark trilayers along the c axis existing every 7 Å in the low-T phase. The modulation of the intensity is more qualitatively seen in the graph at each side of the images, where the intensity integrated along the a axis is plotted.

Figure 4(a) shows the optical conductivity spectra for $Ba_2Ti_{23}O_{22}$ along the a axis [$\sigma_a(\omega)$] and b axis [$\sigma_b(\omega)$] at room temperature, together with those for $BaV_{10}O_{15}$ with a similar structure (a bilayer version of 2-13-22 structure) but having V ions [6]. It is notable that for both compounds three peaks, at ~0.5, 2.5, and 4.5 eV, exist in the spectra. For $BaV_{10}O_{15}$, these peaks were assigned to the transition from V^{2+} to V^{3+} (the excitation to the so-called in-gap state), from V^{3+} to V^{3+} (Mott excitation), and from O^{2-} to V^{3+} (charge-transfer excitation), respectively. For $Ba_2Ti_{23}O_{22}$, the peak for the Mott excitation (~ 2.5 eV) is discernibly smaller, but the peak of the in-gap state (~ 0.4 eV) is larger than that of $BaV_{10}O_{15}$. Namely, the Mott gap (from Ti^{3+} to Ti^{3+}) is collapsed, and more spectral weight is transferred to the in-gap state (from Ti^{3+} to Ti^{4+}) in $Ba_2Ti_{23}O_{22}$. As can be seen in Figs. 4(c) and 4(d), below the peak at 0.4 eV, a Drude-like spectrum exists below 0.1 eV for both $\sigma_a(\omega)$ and $\sigma_b(\omega)$. These results are consistent with the fact that the electrical resistivity and Pauli paramagnetic susceptibility of $Ba_2Ti_{13}O_{22}$ are smaller than those of $BaV_{10}O_{15}$.

As seen in Figs. 4(c) and 4(d), with decreasing T, the Drude-like response for $\hbar\omega < 0.1$ eV and the lower-energy tail of the in-gap excitation spectra for $\hbar\omega < 0.3$ eV are suppressed. However, as seen in Fig. 2(b), where the reflectivity spectra [$R(\omega)$] at 5 and 300 K are plotted (left axis), $R(\omega)$ at 5 K is suppressed for $\hbar\omega \sim 0.1$ eV, but it increases again for lower $\hbar\omega$ and merges with the $R(\omega)$ at 300 K for $\hbar\omega < 0.02$ eV with both $\boldsymbol{E} \parallel a$ (R_a) and $\boldsymbol{E} \parallel b$ (R_b). This behavior is different from that of $R(\omega)$ when a real gap (with the value E_g) opens in the optical conductivity spectrum, where $R(\omega)$ is suppressed for $\hbar\omega < E_g$ down to $\hbar\omega =$ 0 eV. Instead, the behavior shown in Fig. 2(b) suggests the existence of a low-energy Drude component inside the

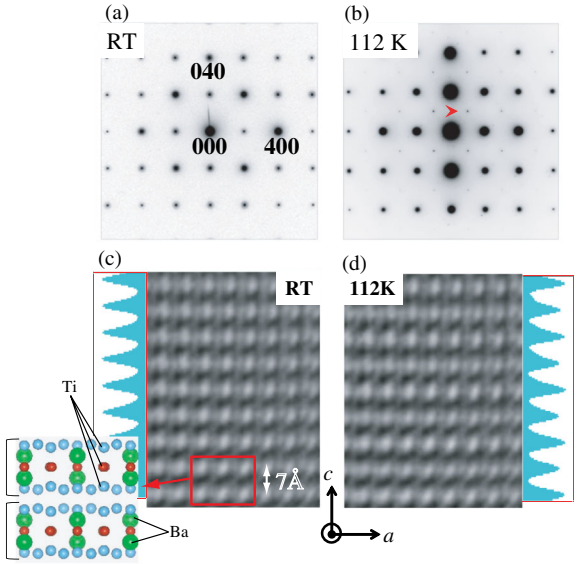

FIG. 3 (color online). (a), (b) Electron diffraction patterns of $Ba_2Ti_{13}O_{22}$ taken from the [001] direction at (a) room temperature and (b) 112 K. (c), (d) High-resolution lattice image of $Ba_2Ti_{13}O_{22}$ at (c) room temperature and (d) 112 K. The graph at each side indicates the integrated intensity along the a direction.

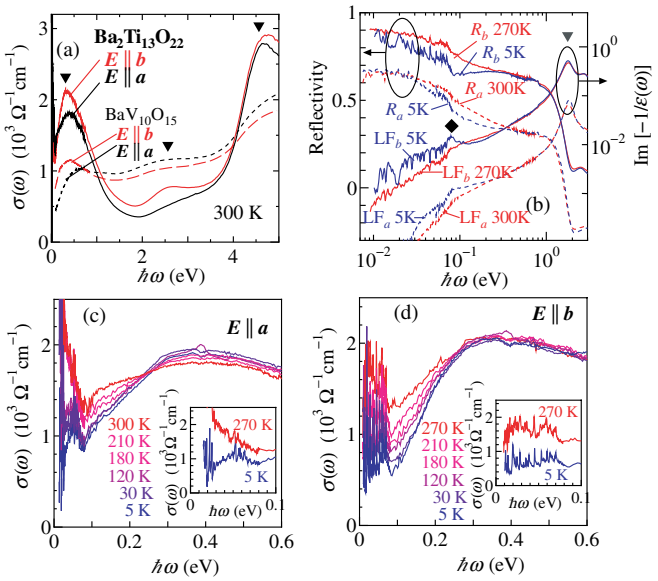

FIG. 4 (color online). (a) Comparison of the optical conductivity $\sigma(\omega)$ between $Ba_2Ti_{13}O_{22}$ (solid lines) and $BaV_{10}O_{15}$ (dashed lines). (b) Reflectivity (R, left axis) and energy loss function (LF, right axis) for $Ba_2Ti_{13}O_{22}$ at 270 and 5 K for $\boldsymbol{E} \parallel a$ (dashed lines) and $\boldsymbol{E} \parallel b$ (solid lines). (c), (d) Optical conductivity spectra for $Ba_2Ti_{13}O_{22}$ at various temperatures for (c) $\boldsymbol{E} \parallel a$ and (d) $\boldsymbol{E} \parallel b$. The insets are expanded figures below 0.1 eV. Sharp peaks existing below 0.1 eV correspond to optical phonon modes.

pseudogap. This is more clearly seen in $\mathrm{Im}[-1/\epsilon(\omega)]$ [right axis of Fig. 2(b)], called the energy loss function, which corresponds to the excitation of the longitudinal modes [21]. The evolution of a peak at ~0.1 eV shown by a rhombus, which corresponds to the longitudinal excitation of the Drude component, is clearly observed in $\mathrm{Im}[-1/\epsilon(\omega)]$ at 5 K for both $\boldsymbol{E} \parallel a$ (LF_a) and $\boldsymbol{E} \parallel b$ (LF_b), in addition to a peak at ~2 eV shown by a triangle, which corresponds to the longitudinal excitation of the in-gap state at 0.4 eV in $\sigma(\omega)$. A Drude peak in $\sigma(\omega)$ (corresponding to the transverse mode of it) should exist at lower than the experimental range ($\hbar\omega < 0.01$ eV) and dominates the behavior the dc resistivity below T_c.

Based on these experimental results, let us discuss the possible origin of the phase transition in $Ba_2Ti_{13}O_{22}$ at ~200 K. First, there is a clear difference from the phase transition in the vanadates with similar crystal structures, $Ba_2V_{13}O_{22}$, or its bilayer version, $BaV_{10}O_{15}$, where V trimerization with V orbital ordering occurs below T_c and $\rho(T)$ diverges at the lowest T. The present $Ba_2Ti_{13}O_{22}$ remains metallic even below T_c, and this experimental result resembles that of charge-density-wave (CDW) states [22]. The existence of both electrons and holes observed in the Hall measurement is consistent with the CDW formation, which causes a reconstruction of the Fermi surface due to the opening of a CDW gap and likely leads to the existence of both hole and electron pockets below T_c. The T dependence of the optical conductivity $\sigma(\omega)$, i.e., the opening of a pseudogap (~ 0.2 eV) and the evolution of a Drude component inside the pseudogap below T_c, also resembles that observed in the CDW transition [21,23].

However, there are several experimental results that are not consistent with a simple CDW picture. First, a conventional CDW transition is caused by the nesting of the Fermi surface, and the period of the CDW usually becomes incommensurate against the unit cell, whereas the charge modulation below T_c is commensurate in $Ba_2Ti_{13}O_{22}$, as shown by electron diffraction measurements. The commensurate order in $Ba_2Ti_{13}O_{22}$ suggests that the ordering has a more localized character, such as charge ordering as observed in perovskite manganites [24]. However, this contradicts the metallic character in the transport properties of the present compound. Second, the behavior of the magnetic susceptibility $\chi(T)$ is different from that of the conventional CDW state. In usual CDW compounds, $\chi(T)$ is T independent (Pauli paramagnetism) above T_c and is suppressed immediately below T_c [25] caused by the disappearance of a part of the Fermi surface, and then it becomes T independent again at lower T. However, in $Ba_2Ti_{13}O_{22}$, $\chi(T)$ keeps on decreasing almost linearly with T below T_c. It should be pointed out that such a T dependence of χ is similar to that of iron pnictide superconductors [26]. Finally, the anisotropy of the electrical resistivity in $Ba_2Ti_{13}O_{22}$ is ~3, which is much smaller than that observed in conventional CDW compounds.

At present, we do not understand what the ground state of $Ba_2Ti_{13}O_{22}$ is, and further experimental and theoretical studies will be necessary for the full understanding of it. Here, we show several theoretical models of the exotic ground states that resemble a CDW state. One is an ordered state with spontaneous orbital currents [27,28]. This can be regarded as a density-wave state of nonzero angular momentum and is favored by spin-orbit coupling. Another one is an excitonic insulator [29,30], where holes and electrons arising from a semimetallic state form excitons and yield a gap in the density of states. In both cases, we expect a commensurate order at low temperatures, consistent with the present experimental results.

In conclusion, we found that $Ba_2Ti_{13}O_{22}$ with Ti^{3+} ($3d^1$) ions on a triangle-based lattice exhibits a phase transition at ~200 K, where electrical resistivity increases but regains a metallic conduction with further lowering temperatures. In the low-T phase, (i) a modulation of the crystal structure appears, (ii) a pseudogap is formed in the density of states, but a remnant Drude component exists inside the pseudogap, and (iii) both electrons and holes contribute to the electrical conduction. These results suggest a CDW state as the ground state of $Ba_2Ti_{13}O_{22}$. However, the commensurate wave vector of the structural modulation and the linear T dependence of the magnetic susceptibility in the low-T phase do not seem compatible with such a simple CDW picture but suggest a novel ground state.

We appreciate S. Uchida for his useful comments. This work was supported by a Grant-in-Aid for Scientific Research B (No. 21340105) from JSPS. The synchrotron radiation experiments were performed at BL44B2 in SPring-8 with the approval of RIKEN (Proposal No. 20100034).

*To whom correspondence should be addressed.
katsuf@waseda.jp

[1] Y. Ren, T. T. M. Palstra, D. I. Khomskii, E. Pellegrin, A. A. Nugroho, A. A. Menovsky, and G. A. Sawatzky, Nature (London) **396**, 441 (1998).
[2] S. Miyasaka, Y. Okimoto, M. Iwama, and Y. Tokura, Phys. Rev. B **68**, 100406(R) (2003).
[3] T. Suzuki, M. Katsumura, K. Taniguchi, T. Arima, and T. Katsufuji, Phys. Rev. Lett. **98**, 127203 (2007).
[4] E. M. Wheeler, B. Lake, A. T. M. Nazmul Islam, M. Reehuis, P. Steffens, T. Guidi, and A. H. Hill, Phys. Rev. B **82**, 140406(R) (2010).
[5] H. F. Pen, J. van den Brink, D. I. Khomskii, and G. A. Sawatzky, Phys. Rev. Lett. **78**, 1323 (1997).
[6] T. Kajita, T. Kanzaki, T. Suzuki, J. E. Kim, K. Kato, M. Takata, and T. Katsufuji, Phys. Rev. B **81**, 060405(R) (2010).
[7] J. Miyazaki, K. Matsudaira, Y. Shimizu, M. Itoh, Y. Nagamine, S. Mori, J. E. Kim, K. Kato, M. Takata, and T. Katsufuji, Phys. Rev. Lett. **104**, 207201 (2010).
[8] M. Ikeda, Y. Nagamine, S. Mori, J. E. Kim, K. Kato, M. Takata, and T. Katsufuji, Phys. Rev. B **82**, 104415 (2010).

[9] K. Takubo, T. Kanzaki, Y. Yamasaki, H. Nakao, Y. Murakami, T. Oguchi, and T. Katsufuji, Phys. Rev. B **86**, 085141 (2012).
[10] H. Nakao, Y. Wakabayashi, T. Kiyama, Y. Murakami, M. V. Zimmermann, J. P. Hill, D. Gibbs, S. Ishihara, Y. Taguchi, and Y. Tokura, Phys. Rev. B **66**, 184419 (2002).
[11] K. Takubo, M. Shimuta, J. E. Kim, K. Kato, M. Takata, and T. Katsufuji, Phys. Rev. B **82**, 020401(R) (2010).
[12] M. Isobe and Y. Ueda, J. Phys. Soc. Jpn. **71**, 1848 (2002).
[13] M. Schmidt, W. Ratcliff II, P. G. Radaelli, K. Refson, N. M. Harrison, and S. W. Cheong, Phys. Rev. Lett. **92**, 056402 (2004).
[14] D. I. Khomskii and T. Mizokawa, Phys. Rev. Lett. **94**, 156402 (2005).
[15] J. Akimoto, Y. Gotoh, K. Kawaguchi, and Y. Oosawa, J. Solid State Chem. **113**, 384 (1994).
[16] K. Kataoka, N. Kijima, H. Hayakawa, A. Iyo, K. Ohshima, and J. Akimoto, J. Solid State Chem. **184**, 3117 (2011).
[17] K. Kato, R. Hirose, M. Takemoto, S. Ha, J. Kim, M. Higuchi, R. Matsuda, S. Kitagawa, and M. Takata, AIP Conf. Proc. **1234**, 875 (2010).
[18] Y. Okada, T. Arima, Y. Tokura, C. Murayama, and N. Mori, Phys. Rev. B **48**, 9677 (1993).
[19] Possible reasons that the x-ray powder diffraction cannot detect such additional peaks are as follows. (i) Because of the large back ground, the x-ray powder diffraction measurement can detect only the peaks with at least 10^{-3} the intensity of the largest ones, and this is much poorer sensitivity than that of the electron diffraction. (ii) The high-resolution transmission electron microscope images that we took indicate the formation of a nanodomain structure in the $C2/m$ phase. The electron diffraction measurement can pick up a signal from one domain in such a multidomain structure, whereas x-ray diffraction measurement detects the average data of many domains, in which the effective intensity is further reduced.
[20] In the $C2/m$ phase, the b axis is the unique axis of the monoclinic lattice and is originally the a axis in the $Cmce$ phase. The a axis of the $C2/m$ phase is originally the b axis in the $Cmce$ phase. The c axis is unchanged.
[21] G. Li, W. Z. Hu, D. Qian, D. Hsieh, M. Z. Hasan, E. Morosan, R. J. Cava, and N. L. Wang, Phys. Rev. Lett. **99**, 027404 (2007).
[22] G. Grüner and A. Zettl, Phys. Rep. **119**, 117 (1985).
[23] A. Sacchetti, L. Degiorgi, T. Giamarchi, N. Ru, and I. R. Fisher, Phys. Rev. B **74**, 125115 (2006).
[24] Y. Tokura and N. Nagaosa, Science **288**, 462 (2000).
[25] F. J. DiSalvo, J. V. Waszczak, and K. Yamaya, J. Phys. Chem. Solids **41**, 1311 (1980).
[26] G. R. Stewart, Rev. Mod. Phys. **83**, 1589 (2011).
[27] C. Nayak, Phys. Rev. B **62**, 4880 (2000).
[28] V. Scagnoli, U. Staub, Y. Bodenthin, R. A. de Souza, M. García-Fernández, M. Garganourakis, A. T. Boothroyd, D. Prabhakaran, and S. W. Lovesey, Science **332**, 696 (2011).
[29] W. Kohn, Phys. Rev. Lett. **19**, 439 (1967).
[30] H. Cercellier *et al.*, Phys. Rev. Lett. **99**, 146403 (2007).
[31] K. Momma and F. Izumi, J. Appl. Crystallogr. **41**, 653 (2008).